Journal of Materials Chemistry A

# Ester-Functionalized, Wide-Bandgap Derivatives of PM7 for Simultaneous Enhancement of Photovoltaic Performance and Mechanical Robustness of All-Polymer Solar Cells



| | |
|---|---|
| Journal: | *Journal of Materials Chemistry A* |
| Manuscript ID | TA-ART-11-2020-011320.R1 |
| Article Type: | Paper |
| Date Submitted by the Author: | 18-Dec-2020 |





| | |
|---|---|
| Complete List of Authors: | You, Hoseon; KAIST,<br>Jones, Austin; Georgia Institute of Technology<br>Ma, Boo Soo; Korea Advanced Institute of Science and Technology, Mechanical Engineering<br>Kim, Geon-U; Korea Advanced Institute of Science and Technology, Chemical and Biomolecular Engineering<br>Lee, Seungjin; Korea Advanced Institute of Science and Technology, Chemical and Biomolecular Engineering<br>Lee, Jin-Woo ; Korea Advanced Institute of Science and Technology, Chemical and Biomolecular Engineering<br>Kang, Hyunbum; KAIST, Department of Chemical and Biomolecular Engineering<br>Kim, Taek-Soo; KAIST, Mechanical Engineering<br>Reynolds, John; Georgia Institute of Technology, Chemistryand Biochemistry, Materials Science and Engineering<br>Kim, Bumjoon; KAIST, Chemical and Biomolecular Engineering |
| | |

# Ester-Functionalized, Wide-Bandgap Derivatives of PM7 for Simultaneous Enhancement of Photovoltaic Performance and Mechanical Robustness of All-Polymer Solar Cells

*Hoseon You[a], Austin L. Jones[b], Boo Soo Ma[c], Geon-U Kim[a], Seungjin Lee[a], Jin-Woo Lee[a], Hyunbum Kang[a], Taek-Soo Kim[c], John R. Reynolds[b,*], and Bumjoon J. Kim[a,*]*

[a] Department of Chemical and Biomolecular Engineering, Korea Advanced Institute of Science and Technology (KAIST), Daejeon 34141, Republic of Korea

[b] School of Chemistry and Biochemistry, School of Materials Science and Engineering, Center for Organic Photonics and Electronics, Georgia Tech Polymer Network, Georgia Institute of Technology, Atlanta, Georgia 30332, United States.

[c] Department of Mechanical Engineering, Korea Advanced Institute of Science and Technology (KAIST), Daejeon 34141, Republic of Korea

**Keywords**: all-polymer solar cells, benzodithiophene polymer donors, ester alkyl side chains, mechanical robustness, stretchability

* Electronic e-mail: bumjoonkim@kaist.ac.kr, reynolds@chemistry.gatech.edu

## Abstract

In this study, two wide-bandgap PM7 polymer derivatives are developed via simple structural modification of the fused-accepting unit by incorporating ester groups on terthiophene at different positions (i.e., two ester groups on the outer thiophenes (PM7 D1) and on the central thiophene (PM7 D2)). This simple modification creates a higher-energy light absorption window, providing better complementary light harvesting with naphthalenediimide-based acceptor, P(NDI2HD-Se). As a result, PM7 D1-based all-polymer solar cells (all-PSCs) exhibit a high power conversion efficiency (PCE) of 9.13%, which outperforms that of the PM7-based all-PSC (PCE = 6.93%). Importantly, the ester structural modification has significant impact on the thin-film mechanical ductility and robustness. For example, elongation properties of PM7 D1 and PM7 D2 pristine films are significantly improved by ca. 2.5 times compared to that of PM7. This result is attributed to the flexible ester groups, which are able to effectively compensate for applied stress. The improved ductile properties of PM7 D1 and PM7 D2 also affect the mechanical ductility of the blend films, leading to 1.5-fold increase in crack onset strain compared with that of PM7 blend film. Therefore, we demonstrate that the introduction of ester groups in conjugated polymers provides a simple and promising strategy for future stretchable electronics.

## Introduction

Polymer solar cells (PSCs) have attracted significant attention as one of the promising next generation power sources due to their solution-processability, energy level tunability, and mechanical flexibility.[1-4] Recently, the power conversion efficiency (PCE) of PSCs has dramatically increased to over 18% via the development of a variety of electroactive materials and the optimization of device processing.[5-7] Among various efficient PSC systems, all-polymer solar cells (all-PSCs), consisting of conjugated polymers as both the electron donor ($P_D$) and acceptor ($P_A$), have been recognized as power generators suitable for portable and wearable electronics.[8-11] Due to facile tuning of the absorption and electronic energy levels of both the $P_D$ and $P_A$, further improvement of the PCE can be achieved by enhancing the short-circuit current density ($J_{SC}$) and the open-circuit voltage ($V_{OC}$) simultaneously.[12-16] Also, all-PSCs show intrinsically higher mechanical ductility and robustness due to the presence of tie molecules and entangled networks from long polymer chains, compared to small molecule acceptor-based PSC systems.[17-23]

Naphthalene diimide (NDI)-based conjugated polymers are one family of $P_A$'s that have been extensively studied in all-PSCs due to their high electron affinity and electron mobility.[24-35] However, the NDI-based $P_A$'s such as (i.e., poly{[*N*,*N*'-bis(2-octyldodecyl)-naphthalene-1,4,5,8-bis(dicarboximide)-2,6-diyl]-*alt*-5,5′-(2,2′-bithiophene)} (P(NDI2OD-T2) and poly{[*N*,*N*'bis(2-hexyldecyl)-naphthalene-1,4,5,8-bis(dicarboximide)-2,6-diyl]-*alt*-2,5-selenophene} (P(NDI2HD-Se)) mainly absorb light at specific wavelength ranges near 350 nm and 600-800 nm. Therefore, significant efforts have been made in the development of new wide-bandgap $P_D$ pairs to induce complementary absorption in the range of 400-600 nm as well as desired morphological and electrical properties with NDI-based $P_A$'s.[36, 37] Typical strategies to develop new wide-bandgap $P_D$'s include the synthesis of (i) donor (D)-acceptor

(A) alternating copolymers by a combination of a strong electron donating D moiety and a weak electron accepting A moiety, (ii) random terpolymerization incorporating two different A units, and (iii) bicomponent random copolymerization with a controlled D:A ratio.[38-42] Among them, the random sequence of D and A moieties of both (ii) random terpolymers and (iii) random copolymers could induce crystal defects and energetic disorder, which are often detrimental to their electrical properties in the thin film.[43, 44] Therefore, the design of new regularly sequenced $P_D$'s by modification of either the D or A moiety is important to achieve complementary light absorption with a $P_A$ without sacrificing electrical properties, and thus achieving high-performance all-PSCs. For example, the bandgap and energy levels of PCE10, which is a classic and representative low-bandgap $P_D$ in the PSC community, was successfully modulated by replacing the existing A moiety with new weak accepting units to develop efficient PBDB-T and PTzBI $P_D$'s.[30, 38, 45] However, there are limited choices of wide-bandgap $P_D$'s that match well with NDI-based $P_A$'s in terms of complementary absorption and appropriate energy levels.

Ester-functionalized thiophene derivatives are promising weak electron accepting units suitable for developing wide-bandgap $P_D$'s. Due to the electron-withdrawing effect of the ester group, the $P_D$'s are expected to have: (i) deep-lying highest occupied molecular orbital (HOMO) energy levels, thus resulting in a wide optical bandgap and smaller HOMO-HOMO offset with a $P_A$; (ii) strong electrostatic interactions with adjacent electron-rich atoms to enhance polymer planarity, improving π-π intermolecular interactions and charge transport ability;[46-48] (iii) their structure is simple, allowing easy access by straightforward and scalable synthesis; and (iv) most importantly, it is known that the ester groups act as an internal plasticizer and, therefore, the incorporation of those functional groups can increase the mechanical ductility and flexibility of polymers. Ester-functionalized materials can also act as an effective extender in blend systems and dramatically improve their ductile properties, which

is an important requirement for their application in flexible and wearable solar cell devices.[20, 21, 49-51] Considering that most efficient $P_D$'s (i.e., PBDB-T and PTzBI-Si) contain a rigid and fused ring-based electron-withdrawing unit,[38, 52] we envisioned that replacing this fused ring acceptor with ester-functionalized thiophenes can provide a new structural motif for efficient wide-bandgap $P_D$'s suitable for efficient all-PSCs with high mechanical stability and ductility.

In this work, we investigate two new $P_D$'s (PM7 D1 and PM7 D2) and apply them to NDI-based all-PSCs. These two $P_D$'s are developed based on the structural motif of the efficient poly[(2,6-(4,8-bis(5-(2-ethylhexyl-3-chloro)thiophen-2-yl)-benzo[1,2-*b*:4,5-*b*']dithiophene))-alt-(5,5-(1',3'-di-2-thienyl-5',7'-bis(2-ethylhexyl)benzo[1',2'-*c*:4',5'-*c*']dithiophene-4,8-dione)] (PM7), but they contain an ester-functionalized terthiophene moiety with the esters located at different positions, i.e., two ester chains on the first and third thiophene units, respectively (PM7 D1), and two ester chains on the central thiophene unit (PM7 D2). As the rigid fused-accepting moiety of 5,5-(1',3'-di-2-thienyl-5',7'-bis(2-ethylhexyl)benzo[1',2'-*c*:4',5'-*c*']dithiophene-4,8-dione (BDD) in PM7 is removed and substituted with ester functionality, the bandgaps of both PM7 D1 and PM7 D2 are successfully enlarged compared to that of PM7, which produces complementary light absorption with the P(NDI2HD-Se) $P_A$ in all-PSCs. As a result, the $J_{SC}$ is significantly increased in PM7 D1- and PM7 D2-based all-PSCs compared to that of PM7-based all-PSCs. In particular, the PM7 D1-based all-PSC demonstrates the highest PCE of 9.13% with a $J_{SC}$ value of 13.27 mA cm$^{-2}$, which outperforms the reference PM7-based all-PSC (PCE= 6.93%). The successful enhancement of PCEs in PM7 D1-based all-PSCs is also attributed to their high charge carrier mobilities. Importantly, the PM7 D1- and D2-based pristine and blend thin films exhibit much higher mechanical ductility than the PM7-based thin films, which is mainly attributed to the absence of a rigid fused-accepting unit and the availability of stress relaxation of the ester alkyl side chains in PM7 D1 and PM7 D2. Overall, our work provides a simple and effective molecular design strategy to

develop wide-bandgap $P_D$'s to enhance both the performance and mechanical robustness of all-PSCs.

## Results and Discussion

**Fig. 1** shows the polymer structures, thin-film UV-vis absorption spectra, and energy level alignment of the three different $P_D$'s and $P_A$ used in this study. When designing the new $P_D$'s, we aimed to tune the absorption window and energy level while minimizing the influence on other polymer properties. Accordingly, ester side chains were introduced on terthiophene to realize new wide-bandgap $P_D$'s with a deep-lying HOMO energy level. In addition, it is expected that replacing the rigid fused ring of BDD with flexible functional groups could enhance the intrinsic mechanical flexibility.[53] Two differently modified acceptor monomers of PM7 D1 and PM7 D2 were synthesized following a previous procedure.[54] Polymerization using Stille cross-coupling between 4,8-bis(4-chloro-5-(2-ethylhexyl)thiophen-2-yl)benzo[1,2-*b*:4,5-*b*']dithiophene-2,6-diyl)bis(trimethylstannane) and each acceptor monomer (BDD and two different ester-functionalized derivatives) was performed to isolate PM7, PM7 D1, and PM7 D2, respectively (**Fig. 1a**). Detailed polymerization conditions are described in the Supplementary Information and the chemical structures were confirmed by $^1$H NMR and elemental analysis. The $P_D$'s properties used in this study are summarized in **Table 1**. The number-average molecular weight ($M_n$) and the dispersity ($Đ$) of the $P_A$ used here (P(NDI2HD-Se)) is 98 kg mol$^{-1}$ and 2.7, respectively, and $M_n$ values of all the three $P_D$'s were controlled to be similar (40-50 kg mol$^{-1}$) in order to minimize its effect on their polymer properties (**Fig. S1**). The three $P_D$'s showed onset points of polymer degradation at between 334 and 375 °C in thermogravimetric analysis and no distinct thermal transition was observed in differential

scanning calorimetry (DSC) measurements, indicating that all the three $P_D$'s are mainly amorphous in character (**Fig. S2**).

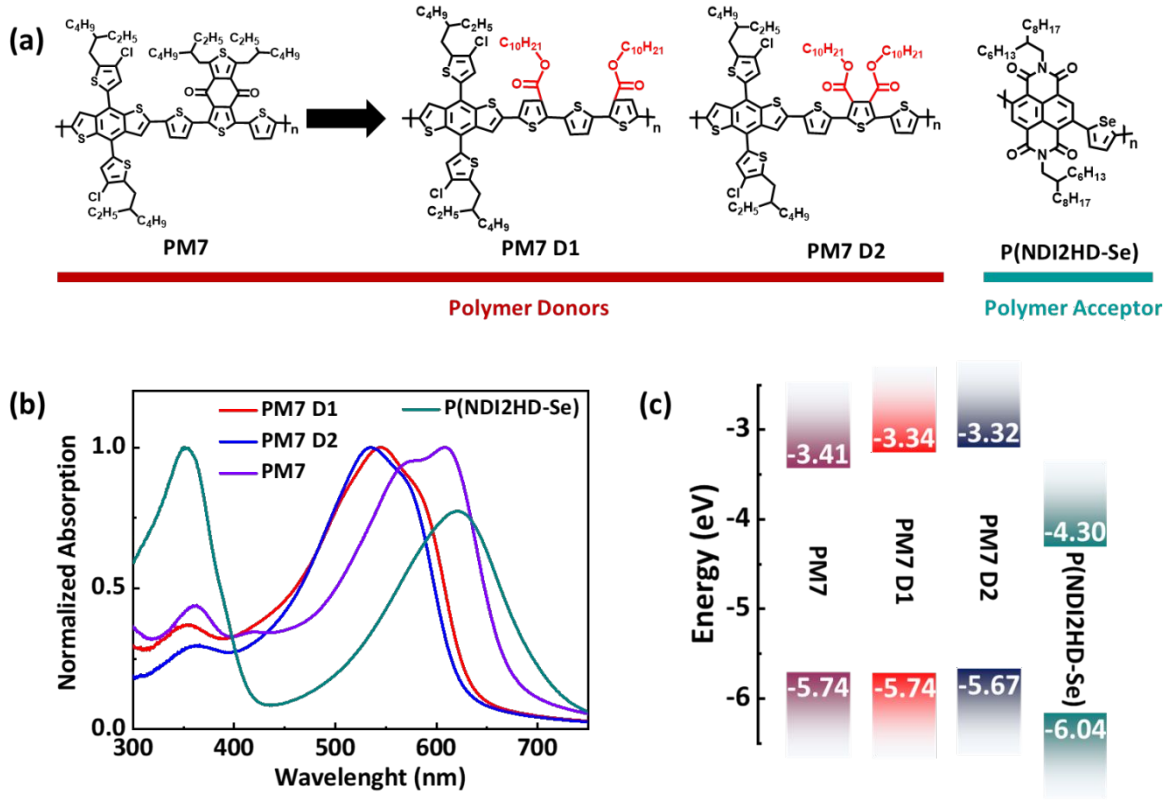


**Fig. 1** (a) Polymer structures, (b) normalized thin-film absorption spectra, and (c) energy level diagram of PM7, PM7 D1, PM7 D2, and P(NDI2HD-Se); the LUMO energy levels of all polymers and HOMO energy levels of $P_D$'s were calculated versus $Fc/Fc^+$ at −5.12 eV. HOMO energy level of $P_A$ was calculated by subtracting optical bandgap from LUMO energy level.

**Table 1** Basic characteristics of $P_D$'s.

| Polymer | $M_n$ (kg mol$^{-1}$) | $Đ$ | $\lambda_{max}$[a)] (nm) | Absorption coefficient[a)] (cm$^{-1}$) | $E_g^{opt}$[a)] (eV) | $E_{HOMO}$[b)] (eV) | $E_{LUMO}$[c)] (eV) | $T_d$ (°C) |
|---|---|---|---|---|---|---|---|---|
| PM7 D1 | 39.6 | 2.7 | 544 | $7.7\times10^4$ | 1.95 | − 5.74 | − 3.34 | 350 |
| PM7 D2 | 45.8 | 2.2 | 535 | $7.8\times10^4$ | 1.98 | − 5.67 | − 3.32 | 334 |
| PM7 | 50.5 | 2.3 | 608 | $7.3\times10^4$ | 1.84 | − 5.74 | − 3.41 | 375 |

[a)] Measured from UV-vis absorption spectra using an as-cast film. [b)] Calculated from onset point of oxidation in DPV curve versus $Fc/Fc^+$ at −5.12 eV. [c)] Calculated from onset point of reduction in DPV curve versus $Fc/Fc^+$ at −5.12 eV.

**Fig. 1b** shows normalized thin-film UV-vis absorption spectra of the three $P_D$'s and $P_A$. All the $P_D$'s show similar absorption coefficients. However, as the BDD acceptor unit was replaced with ester alkyl groups, the absorption profile was blue-shifted from 450-650 nm for PM7 to 400-600 nm for PM7 D1 and PM7 D2. These results are mainly attributed to utilization of oligothiophene functionalized with ester alkyl side chains instead of a fused-accepting moiety.[55] Therefore, PM7 D1 and PM7 D2 exhibit better complementary absorption with P(NDI2HD-Se) compared to that of PM7 due to the blue-shifted absorption spectra, which may contribute to improved $J_{SC}$ in all-PSCs. Next, differential pulsed voltammetry (DPV) was performed on the polymer thin films to estimate their ionization energy (IE) and electron affinity (EA) from the onset potentials (**Fig. 1c**).[54] The first scan of a fresh film was used to estimate the oxidation and reduction potentials to eliminate errors due to changes in film morphology and swelling effects that occur due to repeated electrochemical cycling.[56] The HOMO and lowest unoccupied molecular orbital (LUMO) energy levels of the $P_D$'s and $P_A$ were determined by the onset of oxidation and reduction, respectively (**Fig. S3**). The HOMO/LUMO energy levels of PM7, PM7 D1, and PM7 D2 were estimated to be −5.74/−3.41, −5.74/−3.34, and −5.67/−3.32 eV, respectively. The LUMO energy level of P(NDI2HD-Se) was −4.30 eV obtained from the reduction potential, and the HOMO level of P(NDI2HD-Se) was roughly estimated to be −6.04 eV by subtracting the optical bandgap from the LUMO level. Although this method does not consider the exciton binding energy, it is commonly accepted in the case where oxidation potential is not observed.[57] The DPV measurements show that both PM7 D1 and PM7 D2 have larger bandgaps of 2.40 and 2.35 eV, respectively, compared to that of PM7 (2.33 eV), which agrees with their measured optical bandgap trends (**Fig. 1b**). Here, we note that the IE, and thus the HOMO level, is nearly identical for PM7 and PM7 D1 maintaining small HOMO-HOMO offset with P(NDI2HD-Se),

which suggests their $V_{OC}$ will be similar. On the other hand, PM7 D2's HOMO level is higher which will most likely translate to a lower $V_{OC}$.

Next, PM7 and the two PM7 derivatives were blended with the P(NDI2HD-Se) acceptor to fabricate all-PSCs. Solar cells were fabricated with a conventional device structure of indium tin oxide (ITO)/poly(3,4-ethylenedioxythiophene) polystyrene sulfonate (PEDOT:PSS)/active layer/poly[(9,9-bis(3′-((*N*,*N*-dimethyl)-Nethylammonium)propyl)-2,7-fluorene)-*alt*-5,5′-bis(2,2′-thiophene)-2,6-naphthalene-1,4,5,8-tetracaboxylic-*N*,*N*′-di(2-ethylhexyl)imide]dibromide (PNDIT-F3N-Br)/Ag. The detailed fabrication conditions for each blend system is described in the experimental section. **Fig. 2a** presents the current density–voltage (*J*–V) characteristics measured under AM 1.5G illuminating at 100 mW cm$^{-2}$ and the photovoltaic parameters are summarized in **Table 2**. A histogram of PCEs counts for the devices was plotted with more than 10 device results (**Fig. 2b**), where all the systems showed a Gaussian distribution for PCE with a small standard deviation. The average PCE was found to increase from 6.64% for the PM7-based all-PSC to 8.86% for the PM7 D1-based all-PSC. The champion cell based on PM7 D1:P(NDI2HD-Se) exhibited a PCE of 9.13% with a $V_{OC}$ of 1.00 V, a $J_{SC}$ of 13.27 mA cm$^{-2}$, and a FF of 0.68, which outperformed those of both PM7 and PM7 D2-based all-PSCs. The main reason for the $J_{SC}$ enhancement for the PM7 D1 blend film is the strengthened light harvesting ability in the 400-550 nm region as a result of the blue-shifted absorption profile of PM7 D1, which generates better complementary light absorption with P(NDI2HD-Se). This observation is well-supported by external quantum efficiency (EQE) spectra (**Fig. 2c**). The PM7 D1-based all-PSCs exhibited the highest EQE value of 79% at 500-600 nm. This is important as there are few all-PSC systems reported to date showing a comparably high EQE value of ~ 80%.[52, 58] In the case of PM7 D2-based all-PSCs, the $V_{OC}$ was slightly lower than the other blend systems due to the higher HOMO energy level. Furthermore, despite the blue-shifted absorption of PM7 D2, the enhancement of $J_{SC}$ (11.45 mA cm$^{-2}$) in

PM7 D2-based-all-PSCs was not significant. Rather, the FF value is decreased, resulting in a lower PCE value (6.16%) compared to those of PM7-based and PM7 D1-based all-PSCs. A detailed explanation for the different FF values is provided in the next section. It is evident from the device results that the location of the ester groups in the PM7 backbone led to significantly different photovoltaic behaviours.

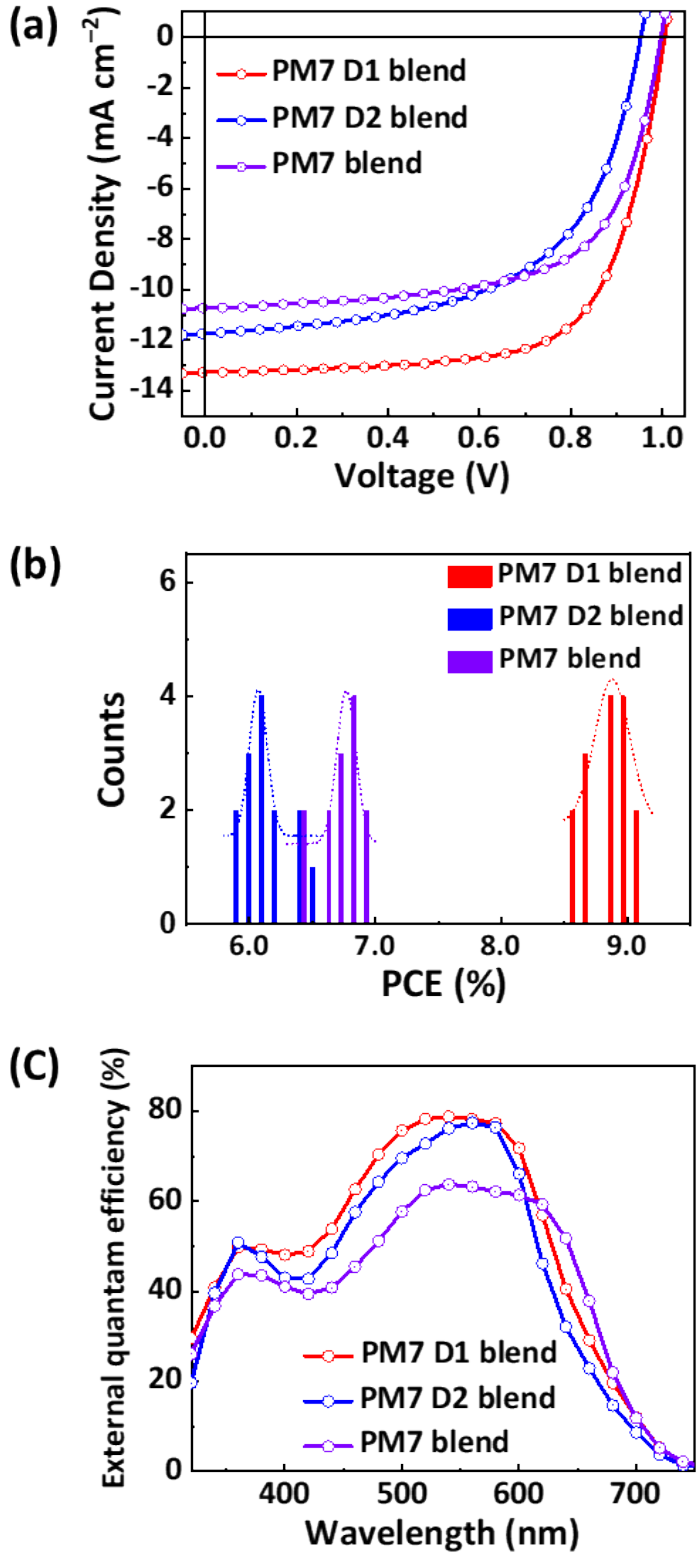


**Fig. 2** (a) *J*–V curves, (b) histogram of counts for PCE, and (c) EQE spectra of the all-PSCs blended with P(NDI2HD-Se) $P_A$.

**Table 2** Photovoltaic performances of all-PSCs blended with P(NDI2HD-Se) $P_A$.

| Active layer | $V_{OC}$ [a)] (V) | $J_{SC}$ [a)] (mA cm$^{-2}$) | FF [a)] (-) | $PCE_{avg}$ [a)] ($PCE_{max}$) (%) |
|---|---|---|---|---|
| PM7 D1 blend | 1.00 ± 0.01 | 13.21 ± 0.27 | 0.67 ± 0.01 | 8.86 ± 0.29 (9.13) |
| PM7 D2 blend | 0.95 ± 0.01 | 11.45 ± 0.48 | 0.56 ± 0.02 | 6.16 ± 0.17 (6.46) |
| PM7 blend | 1.00 ± 0.01 | 10.41 ± 0.26 | 0.64 ± 0.01 | 6.64 ± 0.22 (6.93) |

[a)] The average values were determined from measurements of more than 10 devices.

To probe the differences in the photovoltaic response, we first examined the structural and morphological properties of the three different all-polymer blends by performing grazing incidence wide angle X-ray scattering (GI-WAXS) and resonant soft X-ray scattering (RSoXS) analyses (**Fig. S4**). It was observed in the GI-WAXS results that all the blend films have face-on orientations with (100) peaks at $q_{xy}$= 0.26-0.28 Å$^{-1}$ in the in-plane direction and (010) peaks at $q_z$= 1.70 Å$^{-1}$ in the out-of-plane direction. Also, the crystal coherence length values based on the (100) peaks were estimated for each crystalline blend to be 80-90 Å, indicating similar crystalline characteristics in all of the blend films. When we examined the blend morphology by RSoXS, all the blend films showed similar domain spacing (20-30 nm) (**Fig. S4c**). We selected a photon energy of 284.0 eV for the incident light in the RSoXS measurements, which maximizes material contrast between the different donors and acceptor.[59] Thus, the combined morphological results of GI-WAXS and RSoXS indicate that substituting the BDD moiety with ester-functionalized terthiophenes, and changing the position of the ester groups had no significant influence on their blend morphologies in terms of crystalline ordering, orientation, and the degree of phase separation in the all-polymer blends.

Next, we measured and compared charge mobilities of the blend films using space-charge-limited current (SCLC) measurements (**Table 3**).[60] PM7 D1 and PM7 blend films showed

relatively higher hole mobilities ($\mu_h$) ($1.0 \times 10^{-5}$ and $1.2 \times 10^{-5}$ $cm^2\ V^{-1}\ s^{-1}$, respectively) as compared to that of the PM7 D2 blend film ($0.6 \times 10^{-5}$ $cm^2\ V^{-1}\ s^{-1}$). Higher energetic disorder of PM7 D2 might have caused more unfavorable charge transport ability, which is consistent with the previous report.[54] The lowest $\mu_h$ and relatively unbalanced $\mu_e/\mu_h$ ratio in the PM7 D2-based blend can explain the reason for low FF (below 0.60) as compared to the other all-PSC systems.[61] To investigate the effect of the charge transport abilities on their device performance, free charge recombination and collection behaviours were examined by dependence of $J_{SC}$ on light intensity ($P$) and photocurrent density ($J_{ph}$) against effective voltage ($V_{eff}$), respectively. It is known that $J_{SC}$ follows a power law relationship against $P$ ($J_{SC} \propto P^{\alpha}$), and the slope ($\alpha$) of ln ($J_{SC}$) versus ln ($P$) is close to unity when bimolecular recombination is negligible at short-circuit condition.[62] The PM7 D1 and PM7 blend films showed an $\alpha$ value of almost unity whereas PM7 D2 value was slightly lower (0.95) (**Fig. 3a**). Thus, unlike the cases for both PM7 D1 and PM7 blend films, the PM7 D2 blend film might have suffered from bimolecular recombination and limited the $J_{SC}$ and FF values. Moreover, when we quantitatively investigated the free charge collection behaviour, both PM7 D1 and PM7 blend films showed a higher exciton dissociation probability ($P(E,T)$) with values over 95% as compared to the PM7 D2 blend film (84%) (**Fig. 3b**). Overall, the charge transport and collection properties support the large enhancement of $J_{SC}$ and FF in the PM7 D1-based all-PSCs compared to those of the PM7 D2-based all-PSCs.

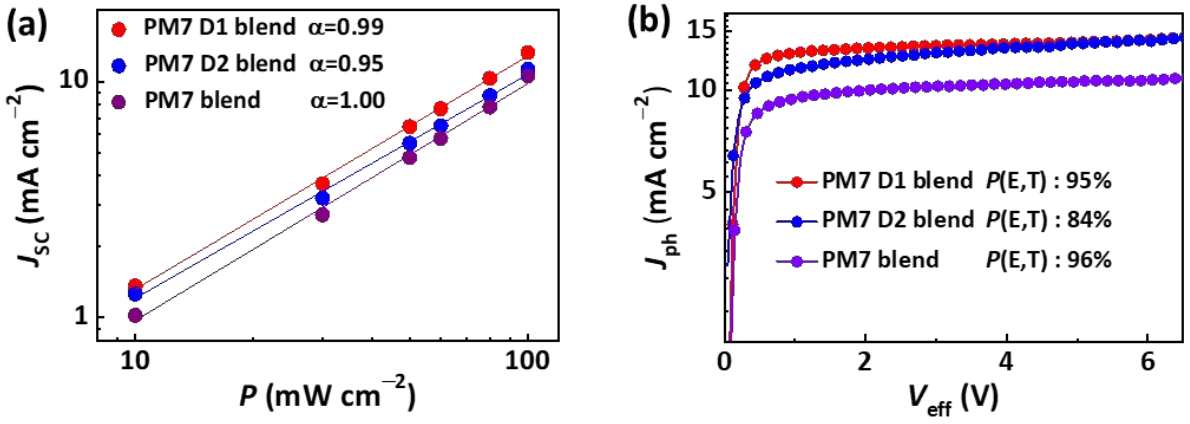


**Fig. 3** (a) Dependence of $J_{SC}$ on light intensity ($P$) and (b) photocurrent analysis of all-PSCs.

**Table 3** SCLC hole and electron mobilities of all-PSCs.

| Active layer | $\mu_h$ (cm$^2$ V$^{-1}$ s$^{-1}$) | $\mu_e$ (cm$^2$ V$^{-1}$ s$^{-1}$) | $\mu_e/\mu_h$ |
|---|---|---|---|
| PM7 D1 blend | $1.0 \times 10^{-5}$ | $3.6 \times 10^{-5}$ | 3.6 |
| PM7 D2 blend | $0.6 \times 10^{-5}$ | $2.9 \times 10^{-5}$ | 4.8 |
| PM7 blend | $1.2 \times 10^{-5}$ | $3.1 \times 10^{-5}$ | 2.6 |

Importantly, in **Fig. 3b**, we note the saturated $J_{ph}$ ($J_{sat}$) value of the PM7 D1 blend film was significantly larger (14.27 mA cm$^{-2}$) compared to that of PM7 (11.08 mA cm$^{-2}$), although they exhibited similar $P(E, T)$ values. To gain deeper insight into the relationship between the light absorption characteristics of the PM7 and PM7 D1-based blend films and their photocurrent generation in all-PSCs, the maximum rate of exciton generation ($G_{max}$) was calculated from a photocurrent analysis and compared. In the saturated regime, the photocurrent is given by $J_{sat} = qG_{max}L$, where $q$ is the electric charge and $L$ is thickness.[63-65] Assuming that all generated excitons are dissociated and collected by an electrode at a high electric field, $G_{max}$ is only governed by the number of absorbed photons. ($G_{max}$ of the PM7 D2 blend was not calculated because $J_{ph}$ value was unsaturated due to its recombination

behaviour.) When we estimated the $G_{max}$ from the above equation, the PM7 D1 blend showed a significantly higher $G_{max}$ value of $9.2\times10^{27}$ $m^{-3}$ $s^{-1}$ than that of PM7 ($7.3\times10^{27}$ $m^{-3}$ $s^{-1}$). Thus, these results indicate that complementary absorption is important to harvest more photons to generate a substantial amount of excitons and subsequent free charges. To investigate how light absorption of the photoactive components contribute to the resulting photocurrent, partial EQE and $J_{SC}$ contributions of donor and acceptor components were estimated and compared for PM7 D1, PM7 D2, and PM7 blend films (**Fig. 4** and **Table 4**).[37, 41] Partial EQE values of the donor and acceptor components in each blend film were calculated from the fractional contribution factor of the donor ($C_D$) and acceptor ($C_A$) absorbance to the total absorbance of each blend film as shown in **Fig. S5** and **Table S1**. The partial photocurrent contributions of the donors and acceptor were determined from integrating the partial EQE of each component multiplied by the AM 1.5G spectrum. The $P_D$'s photocurrent contribution in their respective blend film was improved from PM7 (8.38 mA $cm^{-2}$) to PM7 D2 (8.88 mA $cm^{-2}$), to PM7 D1 (9.47 mA $cm^{-2}$). PM7 D1 exhibited $J_{SC}$ contribution 13% higher than that of PM7. This result can be explained by the enhanced absorption of photons by PM7 D1 and PM7 D2 in the wavelength range of 400-550 nm, where P(NDI2HD-Se) does not competitively harvest light with the $P_D$'s. Therefore, simultaneously achieving a broad light complementary absorption window with efficient charge collection and suppressed recombination is important to realize high-performance all-PSCs with enhanced $J_{SC}$ and FF.

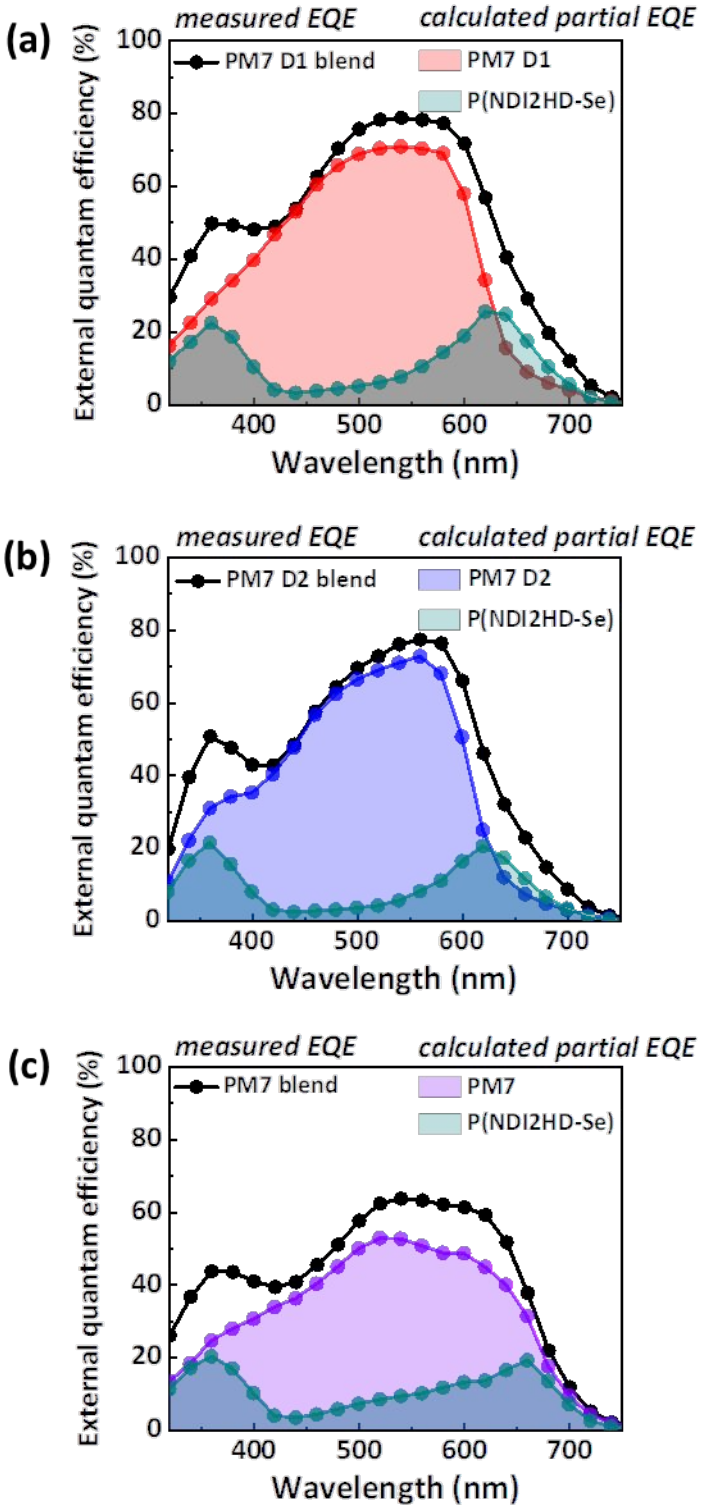


**Fig. 4** Measured EQEs of the blend films and the calculated partial EQEs from each donor and acceptor for the (a) PM7 D1, (b) PM7 D2, and (c) PM7 blend films.

**Table 4** Calculated photocurrent contribution from fractional absorbance of donor and acceptor in the PM7 D1, PM7 D2, and PM7 blend films.

| Active layer | Calculated $J_{SC}$ contribution of donor (mA cm$^{-2}$) | Calculated $J_{SC}$ contribution of acceptor (mA cm$^{-2}$) |
|---|---|---|
| PM7 D1 blend | 9.47 | 2.58 |
| PM7 D2 blend | 8.88 | 1.94 |
| PM7 blend | 8.38 | 2.36 |

Next, we investigated the effect of the $P_D$'s structural modification with regard to the thin-film mechanical properties of the pristine and all-polymer blend films (**Fig. 5** and **Fig. S6**). The blend films were prepared by their optimal conditions for device fabrication, yet without the use of solvent additives and thermal annealing, to elucidate their intrinsic properties. When considering the future applications of PSCs as wearable and stretchable devices and their stability during operation, the importance of tensile properties should be amplified.[3, 18, 20-22, 66] Thus, we evaluated intrinsic tensile properties of the thin films utilizing the pseudo free-standing tensile test which enables measurements without distortion from the effect of a substrate.[19, 67-69] In detail, all the polymer films were initially prepared with a similar thickness of around 100 nm on polystyrenesulfonate (PSS)-coated glass substrates.[67, 68, 70, 71] Since the PSS layer dissolves readily in water, it acts as a sacrificial layer, allowing the polymer thin films to be separated from the glass substrates creating free-standing films by floating them on the surface of water. For PM7 D1 and PM7 D2, ester side chains were introduced to increase the intrinsic chain flexibility due to the elastic characteristics of ester-functionalized polymers.[49, 50, 72] Indeed, we observed that the three $P_D$'s cast as thin films have markedly different tensile behaviours. PM7 exhibited relatively brittle characteristics with high stress over 50 MPa but small crack onset strain (COS) values around 20%. In contrast, the PM7 D1 and PM7 D2 thin films showed highly improved ductile properties with dramatically enhanced

COS values (47% and 58%, respectively). The much higher COS values of PM7 D1 and PM7 D2 originate from the replacement of the fused ring structure of BDD with flexible ester side chains, which can provide possibility of relaxation against applied stresses compared to the rigid BDD moiety in PM7.[50, 53, 72] The slightly higher COS value of PM7 D2, relative to PM7 D1, is likely due to its intrinsic chain flexibility originating from its disrupted backbone planarity by the large steric hindrance of the two closely located ester groups.[20, 73] To support this hypothesis, plane-to-plane angles of the polymer backbones were compared using Spartan 14 package (**Fig. 6**), showing that PM7 D2 has a much larger angle (70°) between the first and third thiophenes than that of PM7 D1 (22°). This large plane-to-plane angle between the adjacent repeating units is expected to bring increased disorder to the polymer chain, increasing the backbone flexibility and ductility of the resulting material.[74]

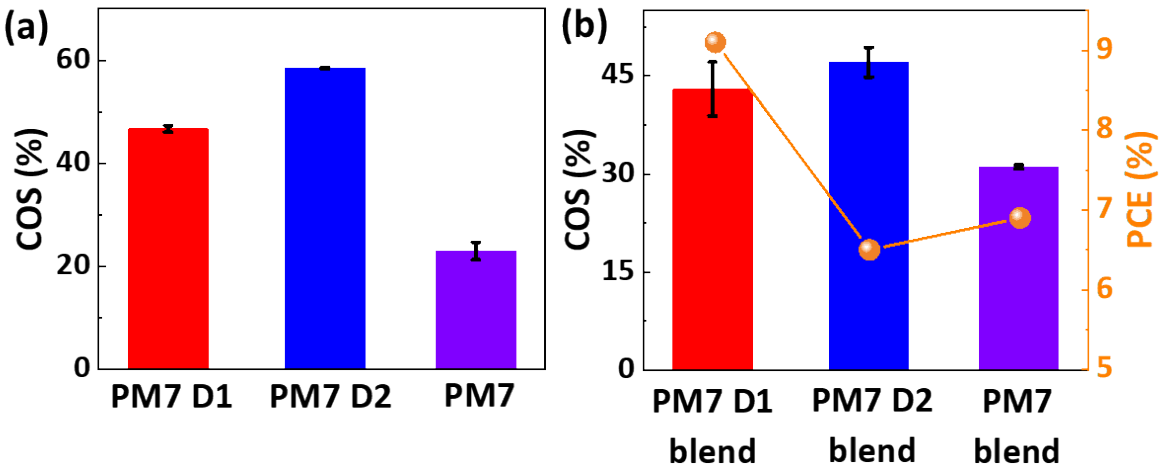


**Fig. 5** COS values of the (a) pristine and (b) blend films (measured by pseudo free-standing tensile test).

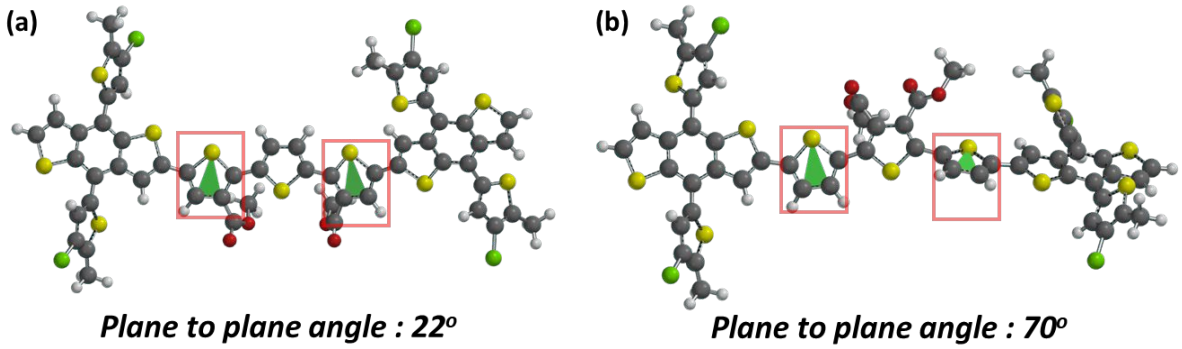


**Fig. 6** Plane-to-plane angle of (a) PM7 D1 and (b) PM7 D2 estimated from density functional theory (DFT) calculation.

A similar trend was observed in the blend films as compared to the pristine film. The PM7 blend films showed moderate ductility with COS values of 31%, while both the PM7 D1 and PM7 D2 blend films showed much increased COSs of 43 and 47%, respectively. This suggests that improvement in ductility of $P_D$'s is highly effective to increase the mechanical robustness of the resulting active layers. To the best of our knowledge, the COS values of the PM7 D1 and PM7 D2 blend films are the highest among the reported all-PSC systems, to date, measured from the free-standing tensile test as summarized in **Table S2**.[17, 18, 75-79] Importantly, we note that PM7 D1 achieved both a high PCE (9.13%) and a COS (43%), which indicates that this blend system demonstrates a promising candidate for commercial applications into flexible and stretchable organic electronics.

## Conclusions

In this work, we reported NDI-based all-PSCs utilizing wide-bandgap PM7 derivatives (PM7 D1 and PM7 D2) as $P_D$'s, and investigated the relationship between their chemical structures and various properties including the photovoltaic performance and mechanical ductility. An ester-functionalized terthiophene was introduced instead of BDD in PM7, and as a result, the absorption windows of PM7 D1 and PM7 D2 were blue-shifted, enabling complementary light absorption with the P(NDI2HD-Se) acceptor. Thereby, a high PCE of 9.13% was achieved in the PM7 D1-based all-PSCs mainly due to the enhanced complementary light harvesting property and desirable charge transport ability. Particularly, substitution of a rigid fused ring with flexible ester alkyl side chains altered the mechanical properties of the conjugated polymer to be more ductile, resulting in much higher COS values in the pristine and blend films. For example, elongation properties of pristine films based-on PM7 D1 and PM7 D2 were significantly improved by ca. 2.5 times compared to that of PM7. As a result, the COS values of the PM7 D1 and PM7 D2 blend films are the highest among the reported PSC systems. Our results highlight the importance of developing the polymer donor with enhanced light absorption and charge transport properties for highly-efficient all-PSCs, and suggest a roadmap for designing conjugated polymers with high mechanical robustness for the application into stretchable organic electronics.

# Experimental

## All-PSC fabrication and characterization

Conventional type all-PSCs with a device structure of ITO/PEDOT:PSS/active layer/ PNDIT-F3N-Br/Ag were fabricated. The ITO-coated glass substrates were cleaned with acetone, deionized water, and finally isopropanol in sonication. Then, the substrates were dried in an oven at 80 °C for 30 min and treated with $O_2$ plasma. Then, the PEDOT:PSS solution was spin-coated on the ITO substrates at 3000 rpm for 40 s with a ramp time of 0.1 s and thermally annealed at 165 °C for 15 min in air. After the films were baked, the substrates were transferred to a nitrogen-filled glove box. The blend solutions of PM7 D1, PM7 D2, and PM7 with P(NDI2HD-Se) in chlorobenzene (17, 17, and 14 mg $mL^{-1}$, respectively) with 1.5 vol% of 1,8-diiodooctane were stirred for 3 h on a hot plate at 80 °C. The donor:acceptor ratio of each blend solution was 2.5:1 (w/w). Then, they were spin-coated onto the ITO/PEDOT:PSS substrates at 2000 rpm for 40 s with a ramp time of 0.1 s. The thicknesses of the blend films were between 90 - 100 nm. After a thermal annealing treatment at 130°C for 10 min, PNDIT-F3N-Br was spin-coated onto the top layers at 2500 rpm for 40 s with a ramp time of 0.1 s.[80] Finally, the Ag electrode (120 nm) was deposited by thermal evaporation under a high vacuum. The active area of the fabricated device was 0.164 $cm^2$, as measured by optical microscopy. The *J*–V curves of the devices were measured using a Keithley 2400 SMU and solar simulator (K201 LAB55, McScience) under irradiance of 100 mW $cm^{-2}$ from a 150 W Xe short-arc lamp filtered by an air mass 1.5 G filter, which satisfies the Class AAA, ASTM Standards. Light intensity was calibrated with a Si reference cell (K801S-K302, McScience). EQE spectra were obtained using a spectral measurement system (K3100 IQX, McScience Inc.). This system was equipped with monochromatic light from a xenon arc lamp at 300 W filtered by an optical chopper (MC 2000 Thorlabs) and a monochromator (Newport). The calculated $J_{SC}$ values were acquired by

integrating the spectra of the EQE with the AM 1.5G solar spectrum, and the calculated values agreed well with the measured $J_{SC}$, within 8% error.

**SCLC measurements**

Hole and electron mobilities of the blend films were acquired by the SCLC method using device structures of ITO/PEDOT:PSS/polymer blends/Au (hole-only) and ITO/ZnO/polymer blends/LiF/Al (electron-only). The blend films were prepared as described in the device fabrication section above. A voltage range of 0-8 V was applied for the current-voltage measurements, and the results were fitted to the Mott-Gurney equation:

$$J_{SCLC} = \frac{9}{8}\varepsilon\varepsilon_0\mu\frac{V^2}{L^3}$$

where $\varepsilon_0$ is the permittivity of free space ($8.85\times10^{-14}$ F cm$^{-1}$), $\varepsilon$ is the relative dielectric constant of the active layer, $\mu$ is the charge carrier mobility, $V$ is the potential across the device ($V = V_{applied} - V_{bi} - V_r$, where $V_{bi}$ is the built-in potential and $V_r$ is the voltage drop caused by the resistance), and $L$ is the thickness of the blend film.

**Estimation of absorption and EQE contributions**

It was assumed that the absorbance of each blend film ($A_B(\lambda)$) can be expressed by the appropriate sum of absorbance of the donor and acceptor components according to Equation 1.[37]

$$A_B(\lambda) = C_D\, A_D(\lambda) + C_A\, A_A(\lambda) \quad (1)$$

where $A_B(\lambda)$ is the absorbance of each blend film, $A_D(\lambda)$ and $A_A(\lambda)$ are normalized absorbance of pristine polymer donor and polymer acceptor films, respectively. $C_D$ and $C_A$ are the wavelength-independent fraction factor of absorbance of donor and acceptor, respectively. We solve the equations 2 and 3 for $C_D$ and $C_A$ using the absorbance normalized to the maximum

absorption peak of the donor and acceptor, $A_D$ and $A_A$. In the case of the PM7 D1 blend film, for example, the $\lambda_{max}$ values of the PM7 D1 and P(NDI2HD-Se) pristine films are 544.5 and 350.5 nm, respectively.

$$A_B(\lambda_{max,\,donor}) = C_D\,A_D(\lambda_{max,\,donor}) + C_A\,A_A(\lambda_{max,\,donor}) \quad (2)$$

$$A_B(\lambda_{max,\,acceptor}) = C_D\,A_D(\lambda_{max,\,acceptor}) + C_A\,A_A(\lambda_{max,\,acceptor}) \quad (3)$$

We assumed that the measured film absorbance is proportional to its absorption coefficient and film thickness, which, in fact, is only valid for thick layers that follow the Beer-Lambert law. However, when a back-reflecting layer is not present, the light absorbance of 100 nm-thick polymer films follows the Beer-Lambert law within a reasonably small deviation, despite the wave-optical coherency expected for thin films.[81] **Fig. S5** displays the absorbance contribution of PM7 D1, PM7, and P(NDI2HD-Se) in the blend films. Then, we use the calculated $C_D$ and $C_A$ to obtain the partial EQEs of donor and acceptor following Equation 4 and 5, respectively.[41] It was assumed that all components have similar internal quantum efficiencies.

$$EQE_D(\lambda) = EQE_{total}(\lambda) \times C_D\,A_D(\lambda) / A_B(\lambda) \quad (4)$$

$$EQE_A(\lambda) = EQE_{total}(\lambda) \times C_A\,A_A(\lambda) / A_B(\lambda) \quad (5)$$

**Pseudo-Free-Standing Tensile Test**

Tensile test of thin films was conducted on water surface. Pristine and blend films were prepared without any treatment in order to see the effect of structural modification. To float the thin films on water, PSS-coated glasses were utilized as the substrates. (Here, the PSS acts as a sacrificial layer. As PSS dissolves in water, the pristine and blend thin films are separated from the glass substrate.) The specimens were patterned in the shape of a dog bone by a femtosecond laser. After floating the patterned specimen, it was gripped by the PDMS-coated

Al grips on the specimen gripping areas. The test of the patterned specimens was performed at a strain rate of ~$0.8 \times 10^{-3}$ $s^{-1}$ until fracture, to obtain the stress-strain curves. All tests were performed under controlled conditions (relative humidity of ~30 % at 25 °C).

## Conflicts of interest

There are no conflicts to declare.

## Acknowledgements

This work was supported by National Research Foundation of Korea (NRF) Grant of the Korean Government (No. 2020R1A4A1018516). B. J. K. acknowledge the support from LG Yonam Foundation of Korea. A. L. J. and J. J. R. acknowledge the support from the Department of the Navy, Office of Naval Research grant number N00014-20-1-2129. This research used resources of The Advanced Light Source, which is a DOE office of Science User Facility under contract No. DE-AC02-05CH11231

## References


1 M. Kaltenbrunner, M. S. White, E. D. Głowacki, T. Sekitani, T. Someya, N. S. Sariciftci and S. Bauer, *Nat. Commun.*, 2012, **3**, 770.

2 G. Wang, F. S. Melkonyan, A. Facchetti and T. J. Marks, *Angew. Chem. Int. Ed.*, 2019, **58**, 4129-4142.

3 C. Lee, S. Lee, G. U. Kim, W. Lee and B. J. Kim, *Chem. Rev.*, 2019, **119**, 8028-8086.

4 B. C. Thompson and J. M. J. Fréchet, *Angew. Chem. Int. Ed.*, 2008, **47**, 58-77.

5 Y. Cui, H. Yao, J. Zhang, T. Zhang, Y. Wang, L. Hong, K. Xian, B. Xu, S. Zhang, J. Peng, Z. Wei, F. Gao and J. Hou, *Nat. Commun.*, 2019, **10**, 2515.

6 Z. Luo, R. Ma, T. Liu, J. Yu, Y. Xiao, R. Sun, G. Xie, J. Yuan, Y. Chen, K. Chen, G. Chai, H. Sun, J. Min, J. Zhang, Y. Zou, C. Yang, X. Lu, F. Gao and H. Yan, *Joule*, 2020, **4**, 1236-1247.

7 C. Zhu, J. Yuan, F. Cai, L. Meng, H. Zhang, H. Chen, J. Li, B. Qiu, H. Peng, S. Chen, Y. Hu, C. Yang, F. Gao, Y. Zou and Y. Li, *Energy Environ. Sci.*, 2020, **13**, 2459-2466.

8 R. Zhao, J. Liu and L. Wang, *Acc. Chem. Res.*, 2020, **53**, 1557-1567.

9 H. Benten, D. Mori, H. Ohkita and S. Ito, *J. Mater. Chem. A*, 2016, **4**, 5340-5365.

10 A. Facchetti, *Mater. Today*, 2013, **16**, 123-132.

11 H. Kang, W. Lee, J. Oh, T. Kim, C. Lee and B. J. Kim, *Acc. Chem. Res.*, 2016, **49**, 2424-2434.

12 K. Feng, J. Huang, X. Zhang, Z. Wu, S. Shi, L. Thomsen, Y. Tian, H. Y. Woo, C. R. McNeill and X. Guo, *Adv. Mater.*, 2020, **32**, 2001476.

13 Y. Guo, Y. Li, O. Awartani, H. Han, J. Zhao, H. Ade, H. Yan and D. Zhao, *Adv. Mater.*, 2017, **29**, 1700309.

14 R. Zhao, N. Wang, Y. Yu and J. Liu, *Chem. Mater.*, 2020, **32**, 1308-1314.

15 W. Wang, Q. Wu, R. Sun, J. Guo, Y. Wu, M. Shi, W. Yang, H. Li and J. Min, *Joule*, 2020, **4**, 1070-1086.

16 Y.-J. Hwang, B. A. E. Courtright, A. S. Ferreira, S. H. Tolbert and S. A. Jenekhe, *Adv. Mater.*, 2015, **27**, 4578-4584.

17 J. Choi, W. Kim, S. Kim, T.-S. Kim and B. J. Kim, *Chem. Mater.*, 2019, **31**, 9057-9069.

18 T. Kim, J.-H. Kim, T. E. Kang, C. Lee, H. Kang, M. Shin, C. Wang, B. Ma, U. Jeong, T.-S. Kim and B. J. Kim, *Nat. Commun.*, 2015, **6**, 8547.

19 W. Kim, J. Choi, J.-H. Kim, T. Kim, C. Lee, S. Lee, M. Kim, B. J. Kim and T.-S. Kim, *Chem. Mater.*, 2018, **30**, 2102-2111.

20 S. E. Root, S. Savagatrup, A. D. Printz, D. Rodriquez and D. J. Lipomi, *Chem. Rev.*, 2017, **117**, 6467-6499.

21 G.-J. N. Wang, A. Gasperini and Z. Bao, *Adv. Electron. Mater.*, 2018, **4**, 1700429.

22 N. Balar, J. J. Rech, R. Henry, L. Ye, H. Ade, W. You and B. T. O'Connor, *Chem. Mater.*, 2019, **31**, 5124-5132.

23 N. Balar, Y. Xiong, L. Ye, S. Li, D. Nevola, D. B. Dougherty, J. Hou, H. Ade and B. T. O'Connor, *ACS Appl. Mater. Interfaces*, 2017, **9**, 43886-43892.

24 N. Zhou and A. Facchetti, *Mater. Today*, 2018, **21**, 377-390.

25 J. W. Jung, J. W. Jo, C.-C. Chueh, F. Liu, W. H. Jo, T. P. Russell and A. K. Y. Jen,

*Adv. Mater.*, 2015, **27**, 3310-3317.

26 Y.-J. Hwang, T. Earmme, B. A. E. Courtright, F. N. Eberle and S. A. Jenekhe, *J. Am. Chem. Soc.*, 2015, **137**, 4424-4434.

27 H. H. Cho, S. Kim, T. Kim, V. G. Sree, S. H. Jin, F. S. Kim and B. J. Kim, *Adv. Energy Mater.*, 2018, **8**, 1701436.

28 S. Feng, C. Liu, X. Xu, X. Liu, L. Zhang, Y. Nian, Y. Cao and J. Chen, *ACS Macro Lett.*, 2017, **6**, 1310-1314.

29 D. Chen, J. Yao, L. Chen, J. Yin, R. Lv, B. Huang, S. Liu, Z. G. Zhang, C. Yang, Y. Chen and Y. Li, *Angew. Chem. Int. Ed.*, 2018, **57**, 4580-4584.

30 C. Lee, H. Kang, W. Lee, T. Kim, K.-H. Kim, H. Y. Woo, C. Wang and B. J. Kim, *Adv. Mater.*, 2015, **27**, 2466-2471.

31 S. Shi, J. Yuan, G. Ding, M. Ford, K. Lu, G. Shi, J. Sun, X. Ling, Y. Li and W. Ma, *Adv. Funct. Mater.*, 2016, **26**, 5669-5678.

32 M. Kim, H. I. Kim, S. U. Ryu, S. Y. Son, S. A. Park, N. Khan, W. S. Shin, C. E. Song and T. Park, *Chem. Mater.*, 2019, **31**, 5047-5055.

33 K. H. Park, Y. An, S. Jung, H. Park and C. Yang, *Energy Environ. Sci.*, 2016, **9**, 3464-3471.

34 X. Liu, C. Zhang, C. Duan, M. Li, Z. Hu, J. Wang, F. Liu, N. Li, C. J. Brabec, R. A. J. Janssen, G. C. Bazan, F. Huang and Y. Cao, *J. Am. Chem. Soc.*, 2018, **140**, 8934-8943.

35 N. Zhou, A. S. Dudnik, T. I. Li, E. F. Manley, T. J. Aldrich, P. Guo, H. C. Liao, Z. Chen, L. X. Chen, R. P. Chang, A. Facchetti, M. Olvera de la Cruz and T. J. Marks, *J. Am. Chem. Soc.*, 2016, **138**, 1240-1251.

36 H. Benten, T. Nishida, D. Mori, H. Xu, H. Ohkita and S. Ito, *Energy Environ. Sci.*, 2016, **9**, 135-140.

37 Z. Li, W. Zhang, X. Xu, Z. Genene, D. Di Carlo Rasi, W. Mammo, A. Yartsev, M. R. Andersson, R. A. J. Janssen and E. Wang, *Adv. Energy Mater.*, 2017, **7**, 1602722.

38 N. B. Kolhe, H. Lee, D. Kuzuhara, N. Yoshimoto, T. Koganezawa and S. A. Jenekhe, *Chem. Mater.*, 2018, **30**, 6540-6548.

39 A. Kim, C. G. Park, S. H. Park, H. J. Kim, S. Choi, Y. U. Kim, C. H. Jeong, W.-S. Chae, M. J. Cho and D. H. Choi, *J. Mater. Chem. A*, 2018, **6**, 10095-10103.

40 L. Gao, Z.-G. Zhang, L. Xue, J. Min, J. Zhang, Z. Wei and Y. Li, *Adv. Mater.*, 2016, **28**, 1884-1890.

41 S. W. Kim, J. Choi, T. T. T. Bui, C. Lee, C. Cho, K. Na, J. Jung, C. E. Song, B. Ma, J. Y. Lee, W. S. Shin and B. J. Kim, *Adv. Funct. Mater.*, 2017, **27**, 1703070.

42 T. E. Kang, K.-H. Kim and B. J. Kim, *J. Mater. Chem. A*, 2014, **2**, 15252-15267.

43 H. Xu, J. Li, J. Mai, T. Xiao, X. Lu and N. Zhao, *J. Phys. Chem. C*, 2014, **118**, 5600-5605.

44 R. Noriega, J. Rivnay, K. Vandewal, F. P. Koch, N. Stingelin, P. Smith, M. F. Toney and A. Salleo, *Nat. Mater.*, 2013, **12**, 1038-1044.

45 B. Fan, L. Ying, Z. Wang, B. He, X.-F. Jiang, F. Huang and Y. Cao, *Energy Environ. Sci.*, 2017, **10**, 1243-1251.

46 H. Sun, T. Liu, J. Yu, T.-K. Lau, G. Zhang, Y. Zhang, M. Su, Y. Tang, R. Ma, B. Liu, J. Liang, K. Feng, X. Lu, X. Guo, F. Gao and H. Yan, *Energy Environ. Sci.*, 2019, **12**, 3328-3337.

47 J. Chen, L. Wang, J. Yang, K. Yang, M. A. Uddin, Y. Tang, X. Zhou, Q. Liao, J. Yu, B. Liu, H. Y. Woo and X. Guo, *Macromolecules*, 2018, **52**, 341-353.

48 Y. Qin, M. A. Uddin, Y. Chen, B. Jang, K. Zhao, Z. Zheng, R. Yu, T. J. Shin, H. Y. Woo and J. Hou, *Adv. Mater.*, 2016, **28**, 9416-9422.

49 K. J. Edgar, C. M. Buchanan, J. S. Debenham, P. A. Rundquist, B. D. Seiler, M. C. Shelton and D. Tindall, *Prog. Polym. Sci.*, 2001, **26**, 1605-1688.

50 A. D. Sagar and E. W. Merrill, *J. Appl. Polym. Sci.*, 1995, **58**, 1647-1656.

51 T. Schauber, S. d. Vos, W. Huhn, B. Rieger and M. Moller, *Macromol. Chem. Phys.*, 1999, **200**, 574-579.

52 Z. Li, L. Ying, P. Zhu, W. Zhong, N. Li, F. Liu, F. Huang and Y. Cao, *Energy Environ. Sci.*, 2019, **12**, 157-163.

53 B. Roth, S. Savagatrup, N. V. de los Santos, O. Hagemann, J. E. Carlé, M. Helgesen, F. Livi, E. Bundgaard, R. R. Søndergaard, F. C. Krebs and D. J. Lipomi, *Chem. Mater.*, 2016, **28**, 2363-2373.

54 A. L. Jones, C. H. Y. Ho, P. R. Riley, I. Angunawela, H. Ade, F. So and J. R. Reynolds, *J. Mater. Chem. C*, 2020, **8**, 15459-15469.

55 S. Li, L. Ye, W. Zhao, H. Yan, B. Yang, D. Liu, W. Li, H. Ade and J. Hou, *J. Am. Chem. Soc.*, 2018, **140**, 7159-7167.

56 A. L. Jones, Z. Zheng, P. Riley, I. Pelse, J. Zhang, M. Abdelsamie, M. F. Toney, S. R. Marder, F. So, J.-L. Brédas and J. R. Reynolds, *Chem. Mater.*, 2019, **31**, 9729-9741.

57 J.-L. Bredas, *Mater. Horiz.*, 2014, **1**, 17-19.

58 L. Zhu, W. Zhong, C. Qiu, B. Lyu, Z. Zhou, M. Zhang, J. Song, J. Xu, J. Wang, J. Ali, W. Feng, Z. Shi, X. Gu, L. Ying, Y. Zhang and F. Liu, *Adv. Mater.*, 2019, **31**, 1902899.

59 L. Ye, X. Jiao, M. Zhou, S. Zhang, H. Yao, W. Zhao, A. Xia, H. Ade and J. Hou, *Adv. Mater.*, 2015, **27**, 6046-6054.

60 Z. Chiguvare and V. Dyakonov, *Phys. Rev. B*, 2004, **70**, 235207.

61 J. D. Kotlarski and P. W. M. Blom, *Appl. Phys. Lett.*, 2012, **100**, 013306.

62 L. J. A. Koster, V. D. Mihailetchi, H. Xie and P. W. M. Blom, *Appl. Phys. Lett.*, 2005, **87**, 203502.

63 V. D. Mihailetchi, H. X. Xie, B. de Boer, L. J. A. Koster and P. W. M. Blom, *Adv. Funct. Mater.*, 2006, **16**, 699-708.

64 J. L. Wu, F. C. Chen, Y. S. Hsiao, F. C. Chien, P. Chen, C. H. Kuo, M. H. Huang and C. S. Hsu, *ACS Nano*, 2011, **5**, 959-967.

65 K.-H. Kim, H. Kang, H. J. Kim, P. S. Kim, S. C. Yoon and B. J. Kim, *Chem. Mater.*, 2012, **24**, 2373-2381.

66 F. C. Krebs, T. D. Nielsen, J. Fyenbo, M. Wadstrøm and M. S. Pedersen, *Energy Environ. Sci.*, 2010, **3**, 512-525.

67 J. Choi, W. Kim, D. Kim, S. Kim, J. Chae, S. Q. Choi, F. S. Kim, T.-S. Kim and B. J. Kim, *Chem. Mater.*, 2019, **31**, 3163-3173.

68 Y. Liu, Y.-C. Chen, S. Hutchens, J. Lawrence, T. Emrick and A. J. Crosby, *Macromolecules*, 2015, **48**, 6534-6540.

69 J. H. Kim, A. Nizami, Y. Hwangbo, B. Jang, H. J. Lee, C. S. Woo, S. Hyun and T. S. Kim, *Nat. Commun.*, 2013, **4**, 2520.

70 R. K. Bay, S. Shimomura, Y. Liu, M. Ilton and A. J. Crosby, *Macromolecules*, 2018,

**51**, 3647-3653.

71 H. Hasegawa, T. Ohta, K. Ito and H. Yokoyama, *Polymer*, 2017, **123**, 179-183.

72 P. Wang and B. Y. Tao, *J. Appl. Polym. Sci.*, 1994, **52**, 755-761.

73 D. Liu, B. Yang, B. Jang, B. Xu, S. Zhang, C. He, H. Y. Woo and J. Hou, *Energy Environ. Sci.*, 2017, **10**, 546-551.

74 J.-S. Kim, J.-H. Kim, W. Lee, H. Yu, H. J. Kim, I. Song, M. Shin, J. H. Oh, U. Jeong, T.-S. Kim and B. J. Kim, *Macromolecules*, 2015, **48**, 4339-4346.

75 Q. Fan, W. Su, S. Chen, W. Kim, X. Chen, B. Lee, T. Liu, U. A. Méndez-Romero, R. Ma, T. Yang, W. Zhuang, Y. Li, Y. Li, T.-S. Kim, L. Hou, C. Yang, H. Yan, D. Yu and E. Wang, *Joule*, 2020, **4**, 658-672.

76 J.-W. Lee, B. S. Ma, J. Choi, J. Lee, S. Lee, K. Liao, W. Lee, T.-S. Kim and B. J. Kim, *Chem. Mater.*, 2019, **32**, 582-594.

77 B. Lin, L. Zhang, H. Zhao, X. Xu, K. Zhou, S. Zhang, L. Gou, B. Fan, L. Zhang, H. Yan, X. Gu, L. Ying, F. Huang, Y. Cao and W. Ma, *Nano Energy*, 2019, **59**, 277-284.

78 W. Lee, J.-H. Kim, T. Kim, S. Kim, C. Lee, J.-S. Kim, H. Ahn, T.-S. Kim and B. J. Kim, *J. Mater. Chem. A*, 2018, **6**, 4494-4503.

79 S. Chen, S. Jung, H. J. Cho, N.-H. Kim, S. Jung, J. Xu, J. Oh, Y. Cho, H. Kim, B. Lee, Y. An, C. Zhang, M. Xiao, H. Ki, Z.-G. Zhang, J.-Y. Kim, Y. Li, H. Park and C. Yang, *Angew. Chem. Int. Ed.*, 2018, **57**, 13277-13282.

80 Z. Wu, C. Sun, S. Dong, X.-F. Jiang, S. Wu, H. Wu, H.-L. Yip, F. Huang and Y. Cao, *J. Am. Chem. Soc.*, 2016, **138**, 2004-2013.

81 C. Cho, S. Jeong and J.-Y. Lee, *J. Opt.*, 2016, **18**, 094001.